Structure and evolution of circumstellar disks during the early phase of accretion from a parent cloud

By Olusola C. Idowu

1. Motivation and Background

The process by which a cloud of gas and dust turns into stars and planets is one of the most intriguing questions in astrophysics. One of the steps in this process is the formation of a disk surrounding a young star. The disk is important because planets may eventually form within it and because it feeds mass to the star. The circumstellar disk has two phases in its evolution. The first is characterized by accretion from the parent cloud directly to the protostar and on to a radially growing disk whose size is comparable to the stellar radius. In the second phase, accretion from the cloud to the disk has ceased. The flow at this later phase of evolution is nearly Keplerian and there is observational data at both mm and infrared wavelengths to provide guidance for theoretical work on the structure of the disk. In contrast, very little is known about the dynamics of the disk in the first phase of evolution because the forming disk is heavily obscured by the parent cloud.

Shu (1977) described the mechanism for the spherically symmetric collapse of an initially isothermal cloud. He suggested that the collapse occurs through the outward propagation of a spherical rarefaction wave. The expanding wave front reduces the support of pressure gradient (against gravity) behind it. This allows gas particles to fall radially inward increasing the mass of the central protostar. For the formation of a disk to take place it is necessary for there to be rotation in the parent cloud. To describe this process Cassen & Moosman (1981), and Terebey, Shu & Cassen (1984) assumed that the cloud collapses in an axisymmetric manner and each gas particles falls with a specific angular momentum $j = rU_\phi$ where r is the radius in cylindrical polar coordinates (Fig. 1) and U_ϕ is the azimuthal velocity. The axis z in Fig. 1 represents the axis of a cylindrical coordinate system. Surfaces of constant angular momentum are represented by nested cylinders. As the rarefaction front propagates, a significant fraction of the infalling gas will possess enough angular momentum so that it can miss the central protostar and become incorporated to the growing disk around the central star. In the present work we consider the evolution of the disk from the time $t_0 = \xi t_*$ where ξ is any positive number and t_* represents the time when the cloud begins to miss the central star defined as

$$t_* = \left(\frac{16 r_*}{\Omega_0^2 a m_0^3}\right)^{1/3}, \tag{1.1}$$

r_* is the initial stellar radius, a is the speed at which the rarefaction front propagates, Ω_0 is the rotation rate of the parent cloud and m_0 is a dimensionless number equal to 0.975 (Terebey, Shu & Cassen (1984)).

If we assume that the total energy in the infalling cloud is small compared to gravitational potential energy (negative), and kinetic energy (positive) at the point of impact-

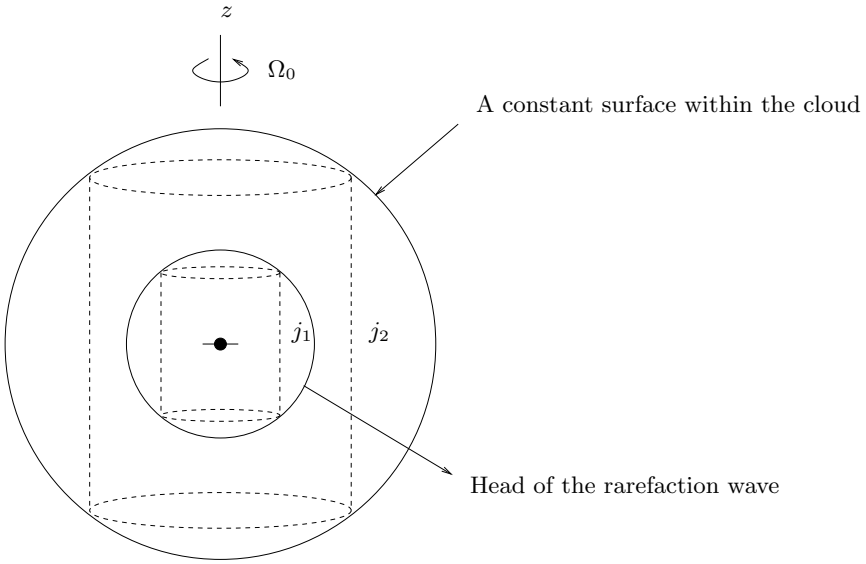

FIGURE 1. Inside-out collapse of a rotating cloud showing the surfaces of constant angular momentum

ing the disk, then the fluid element arrives at a state of essentially free fall. Therefore the streamlines approaching the disk are well approximated by zero-energy orbits, i.e., parabolic trajectories. Cassen & Moosman (1981), Ulrich (1976), and Terebey, Shu & Cassen (1984) have used this basic fact to derive the velocity and density of infalling cloud onto the disk surrounding the central protostar. The velocity for the infalling particle in spherical polar co-ordinates (σ, θ, ϕ) is given by

$$U_\sigma = -\left(\frac{GM}{\sigma}\right)^{1/2}\left(1+\frac{\cos\theta}{\cos\theta_0}\right)^{1/2} \tag{1.2}$$

$$U_\theta = \left(\frac{GM}{\sigma}\right)^{1/2}\left(\frac{\cos\theta_0-\cos\theta}{\sin\theta}\right)\left(1+\frac{\cos\theta}{\cos\theta_0}\right)^{1/2} \tag{1.3}$$

$$U_\phi = \left(\frac{GM}{\sigma}\right)^{1/2}\frac{\sin\theta_0}{\sin\theta}\left(1-\frac{\cos\theta}{\cos\theta_0}\right)^{1/2} \tag{1.4}$$

where θ is the co-latitude and ϕ is the azimuthal angle. The density distribution is given by

$$\rho = -\left(\frac{\dot{M}}{4\pi\sigma^2 U_\sigma}\right)\left[1-\left(1-\frac{\cos\theta}{\cos\theta_0}\right)\left(1-2\cot^2\theta\right)\right]^{-1} \tag{1.5}$$

where the angle θ_0 is the inclination of each orbital plane relative to the rotation axis; it is related to the disk radius R_d by

$$\cos^3\theta_0 - \left(1-\frac{\sigma}{R_d}\right)\cos\theta_0 - \frac{\sigma}{R_d}\cos\theta = 0 \tag{1.6}$$

The disk radius R_d is obtained from Eq. (1.1) at a given t_0 and Ω_0. G is the gravitational constant, M is the mass of the central star, and $\dot{M}$ is the mass accretion rate onto the

star given by

$$\dot{M} = \frac{m_0 a^3}{G} \tag{1.7}$$

(Terebey, Shu & Cassen (1984)). In cylindrical polar coordinates (r, ϕ, z), radial and axial velocities become

$$U_r = -\left(\frac{GM}{r}\right)^{1/2}\left(1 + \frac{\cos\theta}{\cos\theta_0}\right)^{1/2}\left(\frac{1 - \cos\theta\cos\theta_0}{\sin\theta}\right) \tag{1.8}$$

$$U_z = -\left(\frac{GM}{r}\right)^{1/2}\left(1 + \frac{\cos\theta}{\cos\theta_0}\right)^{1/2}\cos\theta_0 \tag{1.9}$$

while U_ϕ remains the same.

Using Eqs. (1.4), (1.5) and (1.8), Stahler *et al* (1994) considered the motion of gas within a vertically mixed thin disk. The thin disk approximation consists of neglecting any variation in the vertical direction.

The goal of the present work is to study via numerical simulation, the processes that occur within the disk as it accretes material. The motion resulting from the infalling streams is assumed to be governed by the Euler equations for compressible gas flow. The main finding so far is that the gas initially within the disk races towards the protostar at supersonic speed to form an equatorial concentration of mass close to the interior boundary of the disk. The mass concentration reduces the radial velocity which in turn diminishes the rate of accretion of gas from the disk to the central protostar from the inner boundary. The flow parameter scaling and the equations of motion used for the simulation are described in the next two sections. Some preliminary results from the flow simulation is discussed in the last section.

2. Non-dimensionalization

Let us begin by denoting all dimensional quantities by tildes. The basic parameters of the problem are the rotation rate of the parent cloud $(\widetilde{\Omega}_0)$, the initial cloud temperature $(\widetilde{T}_0)$, the time since the beginning of the collapse $(\widetilde{t}_0)$, the specific heat capacity of the gas at constant pressure $(\widetilde{c}_p)$, the ratio of specific heats (γ) and the gravitational constant $(\widetilde{G})$. From these basic parameters we can derive other parameter. These are the gas constant $(\widetilde{R} = \widetilde{c}_p(\gamma - 1)/\gamma)$, the initial speed of sound $(\widetilde{a}_0 = \sqrt{\gamma \widetilde{R} \widetilde{T}_0})$, the mass accretion rate $(\widetilde{\dot{M}})$ from Eq. (1.7), and the mass of the central star $(\widetilde{M} = \widetilde{\dot{M}}\widetilde{t}_0)$. The four parameters used to scale the flow are $\widetilde{G}\widetilde{M}$, $\widetilde{c}_p$, $\widetilde{\dot{M}}$ and the initial radius of the disk $\widetilde{R}_d$ obtained from $\widetilde{\Omega}_0$ via Eq. (1.1). The initial conditions of the flow is expressed in these four parameter. Quantities are non-dimensionalized as follows

$$\rho = \frac{\widetilde{\rho}(\widetilde{G}\widetilde{M})^{1/2}\widetilde{R}_d^{3/2}}{\widetilde{\dot{M}}}, \qquad (u_r, u_\theta, u_z) = \frac{(\widetilde{u}_r, \widetilde{u}_\theta, \widetilde{u}_z)}{\widetilde{V}_k} \tag{2.1}$$

$$P = \frac{\widetilde{P}}{\widetilde{\rho}\widetilde{V}_k^2}, \qquad T = \frac{\widetilde{T}\widetilde{c}_p}{\widetilde{V}_k^2}, \qquad \Phi = \frac{\widetilde{\Phi}}{\widetilde{V}_k^2} \tag{2.2}$$

$$r = \frac{\widetilde{r}}{\widetilde{R}_d}, \qquad z = \frac{\widetilde{z}}{\widetilde{R}_d}, \qquad t = \frac{(\widetilde{t} - \widetilde{t}_0)\widetilde{V}_k}{\widetilde{R}_d}, \tag{2.3}$$

where

$$\widetilde{V}_k = \sqrt{\frac{\widetilde{G}\widetilde{M}}{\widetilde{R}_d}}, \tag{2.4}$$

The initial Mach number of the parent cloud is given as

$$Ma = \sqrt{\frac{\widetilde{G}\widetilde{M}}{(\gamma\widetilde{R})\widetilde{R}_d\widetilde{T}_0}} \tag{2.5}$$

Values used for the simulation discussed in this report are $\widetilde{G} = 6.67 \times 10^{-11}\,\mathrm{N.m^2/kg^2}$, $\xi = 3$, $\widetilde{M} = 2 \times 10^{29}\,\mathrm{kg}$ $(0.1M_\odot)$, $\widetilde{R}_d = 2.06 \times 10^{10}\,\mathrm{m}$ (0.14Au), $\widetilde{T}_0 = 20\,K$ (initial cloud temperature), and $\gamma\widetilde{R} = 1.4 \times 10^4\,\mathrm{m^2/(s^2K)}$ (gas constant for molecular Hydrogen). This gives the a cloud rotation rate $\widetilde{\Omega}_0 = 2.6 \times 10^{-14}\,s^{-1}$, mass accretion rate $\widetilde{\dot{M}} = 3.5 \times 10^{-5}\,M_\odot/\mathrm{yr}$ and Mach number $Ma = 48$.

3. Equations of motion and numerical methods of solution

The flow of the gas within the disk is governed by the compressible Euler equations with a gravitational force due to a central point mass:
Continuity equation

$$\frac{\partial\rho}{\partial t} + \frac{1}{r}\frac{\partial}{\partial r}(r\rho u_r) + \frac{1}{r}\frac{\partial}{\partial\theta}(\rho u_\theta) + \frac{\partial}{\partial z}(\rho u_z) = 0 \tag{3.1}$$

Momentum equations

$$\frac{\partial}{\partial t}(\rho u_r) + \frac{1}{r}\frac{\partial}{\partial r}(r\rho u_r^2) + \frac{1}{r}\frac{\partial}{\partial\theta}(\rho u_\theta u_r) + \frac{\partial}{\partial z}(\rho u_r u_z) - \frac{\rho u_\theta^2}{r} = -\frac{\partial P}{\partial r} - \rho\frac{\partial\Phi}{\partial r} \tag{3.2}$$

$$\frac{\partial}{\partial t}(\rho u_\theta) + \frac{1}{r}\frac{\partial}{\partial r}(r\rho u_r u_\theta) + \frac{1}{r}\frac{\partial}{\partial\theta}(\rho u_\theta^2) + \frac{\partial}{\partial z}(\rho u_\theta u_z) + \frac{\rho u_r u_\theta}{r} = -\frac{1}{r}\frac{\partial P}{\partial\theta} \tag{3.3}$$

$$\frac{\partial}{\partial t}(\rho u_z) + \frac{1}{r}\frac{\partial}{\partial r}(r\rho u_r u_z) + \frac{1}{r}\frac{\partial}{\partial\theta}(\rho u_\theta u_z) + \frac{\partial}{\partial z}(\rho u_z^2) = -\frac{\partial P}{\partial z} - \rho\frac{\partial\Phi}{\partial z} \tag{3.4}$$

Energy equation

$$\frac{\partial}{\partial t}(e) + \frac{1}{r}\frac{\partial}{\partial r}(ru_r(e+P)) + \frac{1}{r}\frac{\partial}{\partial\theta}(u_\theta(e+P)) + \frac{\partial}{\partial z}(u_z(e+P)) = 0 \tag{3.5}$$

where

$$e = \frac{\rho T}{\gamma} + \frac{\rho}{2}(u_r^2 + u_\theta^2 + u_z^2) + \rho\Phi \tag{3.6}$$

is the total energy. The gravitational potential term is given as

$$\Phi = -\frac{GM}{(r^2+z^2)^{1/2}} \tag{3.7}$$

As a prelude to proper modeling of radiative cooling, we assumed the flow is isothermal i.e replacing the energy equation with $T = T_0$.

3.1. *Numerical methods, boundary and initial conditions*

The numerical methods used for solving the above equations are similar to those used in studies of compressible jet flow by Freund (1997) and his code was used as a starting

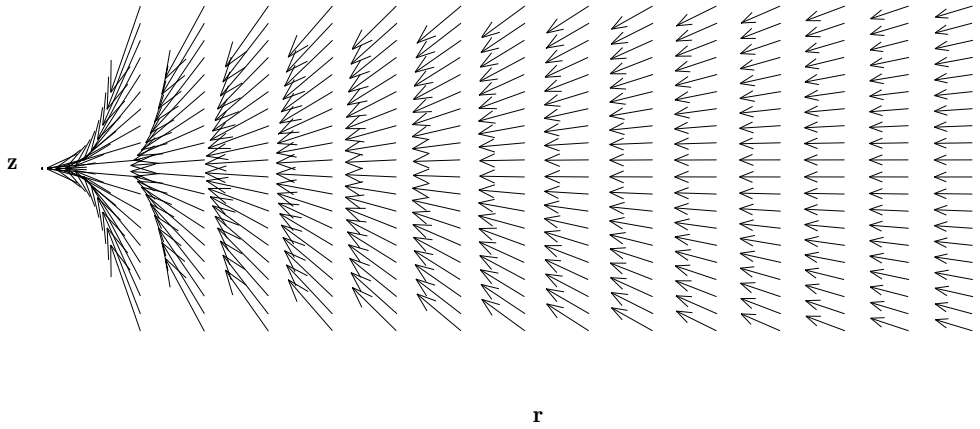

FIGURE 2. Initial velocity in a meridional (zr) plane. The protostar is on the left of the diagram. $(r_{min}, z_{min}) = (0.1, -3.5)$, $(r_{max}, z_{max}) = (2.0, 3.5)$

point. Spatial discretization in all directions was done using the sixth-order Padé-like scheme developed by Lele (1992). The details of the discretization schemes are discussed by Freund (1997). The fourth-order Runge-Kutta method was used for time advancement. To ensure stability we compute a time step based on the Courant-Friedrichs-Lewy (CFL) criterion.

These numerical schemes were tested for different steady-state compressible gas flows: solid body rotation, radially converging flow (nozzle flow), and adiabatic flow of gas in vertical hydrostatic balance between thermal pressure and the z-component of gravity.

At the top, bottom, and outer radial boundaries of the computational domain, the flow may be locally supersonic or subsonic depending on the choice of initial conditions. To determine the local flow at these boundaries, we apply the non-reflecting boundary condition of Giles (1990) using the Cassen and Moosman flow (described earlier) as the reference flow. To start the simulation we need an initial condition which we expect will form a steady or statistically stationary state. For the results shown here we assume that the initial condition is the same as the Cassen and Moosman flow except that to eliminate collisions of gas particles at the midplane of the disk, we diminished the axial velocity Eq. (1.9) to zero at the midplane using the function $f(z) = \tanh(z/\epsilon z_{max})$ where $\epsilon = 0.3$. We did not specify any boundary condition at the inner boundary because the initial Cassen and Moosman flow at this boundary is radially supersonic. We assumed that the gas is initially isothermal. The initial velocity field and density are shown in Figs. 2 and 3 respectively.

4. Results

We observed that the gas initially inside the disk races towards the star to form an equatorial concentration of mass close to the inner boundary of the disk (Fig. 4). The mass concentration significantly reduces the radial velocity within the same region (Figs. 5, 6 and 7). As the simulation progresses, the flow at the inner boundary eventually becomes subsonic, making our assumption of a supersonic outflow at the inner boundary invalid: at this point we stopped the simulation. It is possible that the equatorial concentration

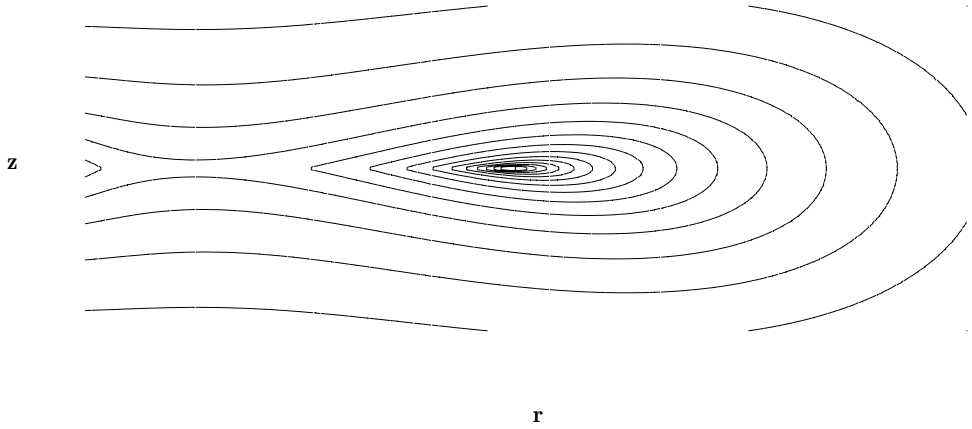

FIGURE 3. Initial log of density contours. The maximum value is 3.024 and the minimum is -0.852. $(r_{min}, z_{min}) = (0.1, -3.5)$, $(r_{max}, z_{max}) = (2.0, 3.5)$

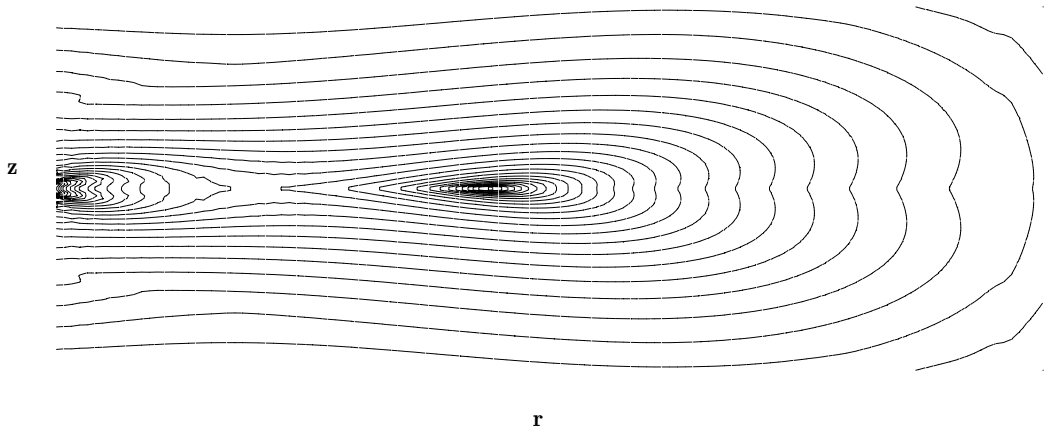

FIGURE 4. Log of density contours in meridional plane showing the equatorial concentration of density at the inner boundary. $(r_{min}, z_{min}) = (0.1, -3.5)$, $(r_{max}, z_{max}) = (2.0, 3.5)$

of mass is a transient behavior and it will eventually be pushed into the protostar when there is sufficient build up of mass within the disk. To answer this question properly we need to adopt a more suitable boundary condition for the inner boundary of the disk. This boundary condition should allow waves propagating from inside the disk to leave the computational domain and disallow any incoming waves. The Giles boundary condition used for the other boundary cannot be used for this because a reference flow at the inner boundary is unknown. The mass flux at the inner boundary of the computational domain ($\dot{M}_{out}$) was reduced significantly (Fig. 8) because of the decreasing radial velocity at the inner boundary. The quantity plotted in Fig. 8 should be unity at steady state. Clearly, the calculation is very far from such a state. Our future research efforts will first concentrate on the processes involved in the approach of a circumstellar disk to steady state and then study instabilities and turbulence evolving from this state.

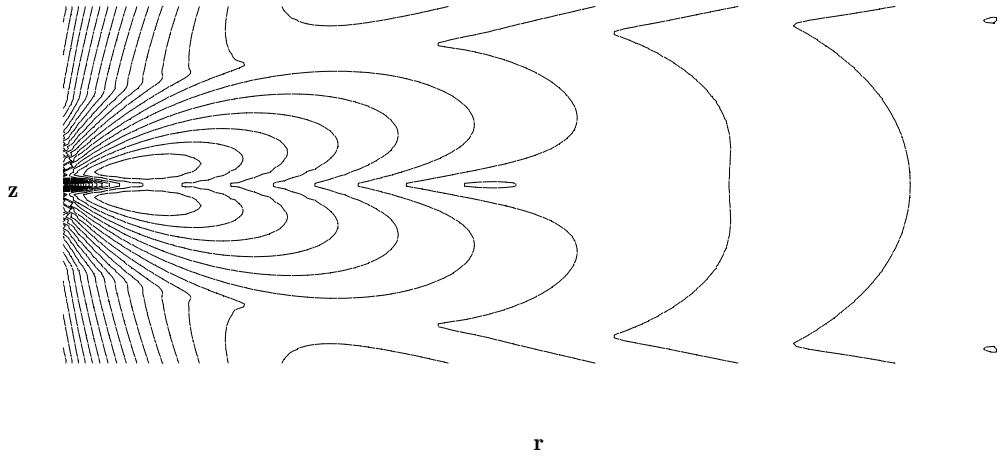

FIGURE 5. Contour plot of the radial velocity at time $t = 0.002$. Co-ordinates of the corners of the computational box are $(r_{min}, z_{min}) = (0.1, -3.5)$, $(r_{max}, z_{max}) = (2.0, 3.5)$

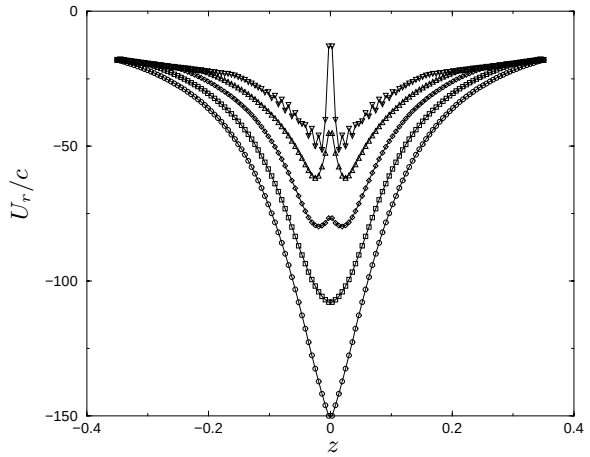

FIGURE 6. Evolution of radial velocity at the inner boundary normalized by the local speed of sound. $\circ : t = 0.0000$; $\square : t = 0.0004$; $\diamond : t = 0.0009$; $\triangle : t = 0.0014$; $\triangledown : t = 0.0019$

Acknowledgments

The author gratefully acknowledges Dr. Karim Shariff and Dr. Steven Stahler for valuable discussions and contributions during the course of this work.

REFERENCES

CASSEN P. & MOOSMAN A. 1981 On the formation of protostellar disks, *ICARUS* **48**, 353–376.

STAHLER S.W., KORYCANSKY D.G., BROTHERS M.J., & TOUMA J 1994 The early evolution of protostellar disks, *Astrophys. J.* **431**, 341–358.

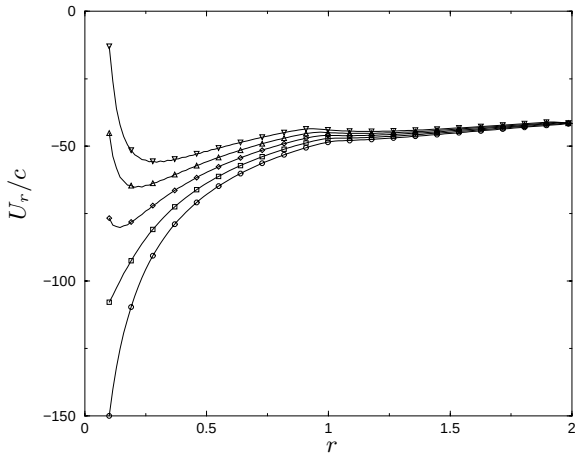

FIGURE 7. Normalized radial velocity at the midplane at different times. ○ : $t = 0.0000$; □ : $t = 0.0004$; ◇ : $t = 0.0009$; △ : $t = 0.0014$; ▽ : $t = 0.0019$

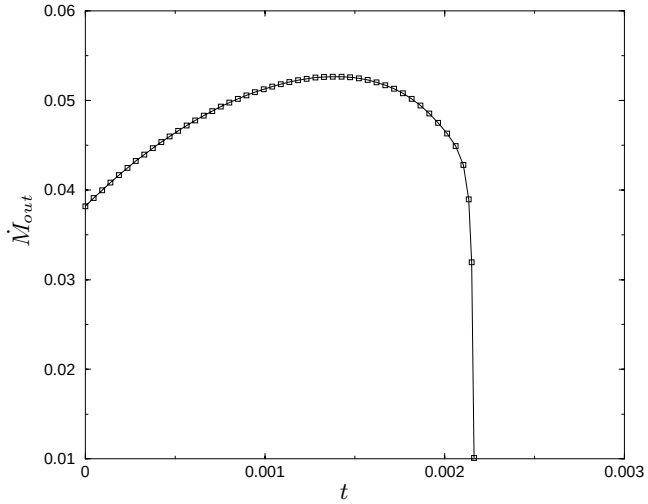

FIGURE 8. Mass flux at the inner radial boundary normalized by the total mass influx into the computational domain.

TEREBEY S., SHU F.H., & CASSEN P. 1984 The collapse of the cores of slowly rotating isothermal clouds, *Astrophys. J.* **286**, 529–551.

SHU F.H. 1977 Self-similar collapse of isothermal spheres and star formation, *Astrophys. J.* **214**, 488–497.

ULRICH, R.K. 1976 An infall model for the T Tauri phenomenon, *Astrophys. J.* **210**, 377–391.

FREUND, J.B., MOIN, P. & LELE, S.K. 1997 Compressibility effects in a turbulent annular mixing layer, *Dept. of Mech. Engr., Stanford University* **Report No. TF–72**

LELE, S.K. 1992 Compact finite difference schemes with spectral-like resolution, *J. Comp. Phys.* **103**, 16–42.

Giles, M.B. 1990 Nonreflecting boundary conditions for Euler equation calculations, *AIAA J.* **18**, 2050–2058.